Structural transformations induced in Fe/Ti multilayers by Ar- and Kr-ion irradiation

2005 J. Phys.: Condens. Matter 17 2149

(http://iopscience.iop.org/0953-8984/17/13/013)

INSTITUTE OF PHYSICS PUBLISHING JOURNAL OF PHYSICS: CONDENSED MATTER

J. Phys.: Condens. Matter **17** (2005) 2149–2165 doi:10.1088/0953-8984/17/13/013

Structural transformations induced in Fe/Ti multilayers by Ar- and Kr-ion irradiation

M Kopcewicz[1], J Jagielski[1,2] and T Stobiecki[3]

[1] Institute of Electronic Materials Technology, Wolczynska 133, 01-919 Warszawa, Poland
[2] The Andrzej Soltan Institute for Nuclear Studies, 05-400 Swierk/Otwock, Poland
[3] Department of Electronics, University of Mining and Metallurgy, Aleja Mickiewicza 30, 30-059 Krakow, Poland

Received 14 December 2004, in final form 3 February 2005
Published 18 March 2005
Online at stacks.iop.org/JPhysCM/17/2149

Abstract

The structural transformations in Fe/Ti multilayers induced by Ar- and Kr-ion irradiation are studied by conversion electron Mössbauer spectroscopy (CEMS). Samples of Ti-to-Fe thickness ratios $\beta = d_{Ti}/d_{Fe} = 1$ (nominal composition $Fe_{0.6}Ti_{0.4}$) and $\beta = 1.5$ ($Fe_{0.5}Ti_{0.5}$) with modulation wavelengths $\Lambda = 10$–60 nm ($\Lambda = d_{Fe} + d_{Ti}$, where d_{Fe} and d_{Ti} are the elemental thickness of Fe and Ti layers) were used. The total thickness of the films was 240 nm. The ion-beam mixing of multilayers was induced by 200 keV Ar^{2+} and 350 keV Kr^{2+} ion irradiation with fluences ranging from 5×10^{13} to 1.3×10^{17} cm^{-2} (Ar) and 0.5×10^{13} to 5.6×10^{16} cm^{-2} (Kr). The ranges of Ar and Kr ions were about 105 and 95 nm, respectively. Ion-beam mixing process leads at low ion fluence to the formation of the solid state solution bcc-FeTi which at higher ion fluences converts to the amorphous FeTi phase. The degree of amorphization depends on the ion fluence, composition of the FeTi system and modulation wavelength. It was noted that the mixing efficiency is considerably larger for heavier ions (Kr as compared with Ar). The relative fractions of given phases were determined from the CEMS measurements. Deterioration of the amorphous phase and partial restoration of the bcc-FeTi solid solution at highest Ar-ion fluences was observed. The results were interpreted based on the enthalpy curves for amorphous FeTi and bcc-FeTi solid solutions.

1. Introduction

Ion irradiation is a powerful method for the surface modification of materials. An ion beam may be used for a direct mass transport leading to compositional changes of the irradiated target. Such a process is called ion implantation. However, the ion beam can serve as an energy carrier only. The energetic ions collide with target nuclei leading to the formation of defects or to the recoil of target atoms. This latter process may induce compositional changes in layered

structures and is called ion-beam mixing. Ion-beam mixing allows the formation of layers of virtually any composition, and the process can be performed at any temperature [1–3]. The intrinsic characteristic of the ion-beam mixing is the high concentration of radiation defects. The process is thus well suited for the formation of metastable amorphous phases [4]. In order to induce such transformation in metallic systems the concentration of foreign atoms must be sufficient to stabilize a disorder created by incoming energetic ions. Taking into account very efficient defect production during irradiation with heavy ions the amorphization process is controlled by mass transport and not by damage creation [5]. The efficiency of mixing, usually defined as the ratio of the increase of the standard deviation of the impurity profile to the fluence increase, depends on the deposition energy density due to nuclear collisions and increases with increasing mass of the ions. In most ion-beam mixing experiments the energy of ions is high enough to assure an ion range comparable with the thickness of the multilayer film deposited on the substrate. The ion fluences required for effective mixing range from 10^{13} to 10^{17} ions cm^{-2}.

The most important mixing mechanisms discussed in the literature are:

(i) ballistic mixing [6] and
(ii) mixing within thermal spikes (overlapping [1] or nonoverlapping [7]).

These processes occur during the evolution of the displacement cascade, i.e. during about 10^{-11} s after ion impact. The atomic redistribution can be assisted by post-cascade transport mechanisms such as radiation-enhanced diffusion (RED [8]) or radiation-induced segregation (RIS [8]). However, the contribution of a given mechanism to the mixing is difficult to determine in practice.

The ion-beam induced amorphization of various metal–metal multilayer thin film systems has been studied extensively in recent years. Numerous empirical rules which define the conditions necessary to obtain amorphization of the multilayer system have been formulated (for a recent review see, for example, [4, 9]). It is advantageous that two constituents of the system have different crystalline structures, the size of both types of atoms differ significantly, and that the system forms stable compounds. These rules are, however, of only limited use in predicting the formation of amorphous phase.

In the present study we used the ion-beam mixing technique to induce the structural transformations leading to the amorphization of the Fe/Ti multilayer system. This system is very well suited for such study because the Liu rules [9] are well fulfilled: the multilayer constituents have different crystalline structures (Fe is bcc and Ti is hcp at room temperature) and the Fe–Ti equilibrium phase diagram reveals two stable intermetallic compounds: cubic FeTi and hcp-Fe_2Ti [10, 11]. Also a bcc-FeTi alloy can be formed [12, 13]. The amorphous FeTi phase is fairly difficult to obtain. The most common technique of rapid quenching from the melt [14–17] is unable to provide the amorphous FeTi phase. As a result of splat cooling from the melt, β-Ti(Fe) or Ti–Fe(Ti) solid solutions with the solubility range enhanced up to 50% have been formed [18]. The amorphous FeTi phase was formed by vapour quenching [15], sputtering [14–16, 19], mechanical alloying [20] and ion implantation [21]. Amorphization of the crystalline Fe/Ti multilayers by ion-beam mixing with Xe ions of energy of 800 keV was also demonstrated [22]. However, the possibility of the formation of the amorphous phase in this way depends strongly on the purity of the Fe and Ti layers and may be prohibited by carbon and oxygen contamination at the interfaces [23].

The Fe/Ti multilayer system is an artificially composition modulated material whose structural and magnetic properties are governed by the thickness of the individual elemental layers. This system is interesting both from the point of view of basic research (magnetic and transport properties) and because of its applications (for example, as a buffer layer

in the giant magnetoresistance sensors [24] and as a hydrogen storage material [25, 26]). Recently, we have studied the microstructure and magnetic properties of Fe/Ti multilayers by using conversion electron Mössbauer spectroscopy (CEMS) and x-ray diffraction (XRD). The magnetization, coercive field and electrical resistivity were measured for multilayers with different compositions and structural modulation wavelengths [19].

It is fairly easy to distinguish the amorphous FeTi phase from the crystalline FeTi and Fe_2Ti compound thanks to the clearly different hyperfine parameters. Mössbauer spectroscopy was successfully used for such studies [14–17, 27]. As shown in [14] and [15], the quadrupole splitting (QS) depends strongly on the iron content in amorphous Fe_xTi_{1-x} alloys for $x < 0.6$ and decreases almost linearly from about 0.36 to 0.29 mm s^{-1} for $x \approx 0.25$ and 0.6, respectively. The QS value remains almost constant for $x \approx 0.6$–0.7 and then increases again to about 0.31 mm s^{-1} for $x \approx 0.8$. The isomer shift (δ) is less sensitive to the alloy composition. It increases from about -0.22 mm s^{-1} for $0.25 \leqslant x \leqslant 0.5$ to about -0.15 mm s^{-1} for $x \approx 0.8$. The bcc-Fe(Ti) alloy is magnetic with a hyperfine field of about 29 T and $\delta \approx 0.02$ mm s^{-1} at room temperature. The formation of such a bcc-Fe(Ti) alloy as a result of Ti-ion implantation into α-Fe has also been observed [28].

In the present study we used the same samples as in [19] for the ion-irradiation experiments. The main characterization technique used for the determination of the structural transformations induced in the Fe/Ti due to ion-beam mixing (interface mixing, phase formation, amorphization) was CEMS supplemented by XRD.

2. Experimental details

Multilayer Fe/Ti films were prepared by rf-sputtering deposition using Fe and Ti targets at a base pressure of 1×10^{-5} Pa. The pressure during sputtering of argon gas was 0.7 Pa and the deposition rates were 0.6 and 0.5 nm s^{-1} for Fe and Ti, respectively. Samples with the two thickness ratios $\beta = d_{Ti}/d_{Fe} = 1.5$ (nominal composition $Fe_{0.5}Ti_{0.5}$) and 1 ($Fe_{0.6}Ti_{0.4}$) were prepared. The elemental thicknesses of both Fe and Ti layers were 5, 10, 20, 30 and 40 nm for $\beta = 1$, and 4, 8, 16, 24 and 32 nm of Fe and 6, 12, 24, 36 and 48 nm of Ti for $\beta = 1.5$. Thus, the modulation wavelengths $\Lambda = d_{Fe} + d_{Ti}$ varied from 10 to 80 nm for both compositions. The total thickness of the film stacks deposited on Corning glass substrate was about 240 nm. The thickness of the elemental layers was measured during deposition with a quartz sensor. In all samples the top layer was composed of Fe.

In order to induce ion-beam mixing the multilayer samples were irradiated at room temperature with 200 keV Ar^{2+} or 350 keV Kr^{2+} ions by using a Balzers MPB 202RP implanter. The ion fluences (Φ) ranged from 5×10^{13} to 1.3×10^{17} Ar atoms cm^{-2} and from 0.5×10^{13} to 5.6×10^{16} Kr atoms cm^{-2}. The beam current density was limited to less than 1 μA cm^{-2} to avoid extensive heating and to keep the target temperature below 50 °C. The ranges of Ar and Kr ions calculated by the TRIM program [29] were about 105 and 95 nm, respectively.

After each irradiation step the samples were analysed by conversion electron Mössbauer spectroscopy (CEMS), the backscatter technique being ideally suited for thin surface layer characterization of Fe-containing materials. Nearly 90% of the CEMS signal comes from about a 120 nm thick surface layer of the sample that coincides well with the thickness of the irradiated layer ($\sim$100 nm). The maximum of the damage distribution induced by incoming ions is located at the depth below the surface of the sample. However, for low ion fluences the difference between the accumulated damage at the sample surface and at the depth at which the maximum damage occurs is less than factor of two, and decreases with irradiation fluence due to sputtering. Consequently, the influence of nonuniform defect distribution can be neglected for fluences varying more than four orders of magnitude.

The CEMS measurements were performed at room temperature by using a He–6% CH_4 gas flow electron counter. A conventional constant acceleration computer controlled Mössbauer spectrometer with a ^{57}Co-in-Rh source was used. The Mössbauer spectral parameters (linewidths, Γ, hyperfine fields, $H_{\rm hf}$, quadrupole splittings, QS, isomer shifts, δ) were determined by fitting Lorentzian line shapes to the experimental data by the least-squares method. The calculations of the hyperfine field distributions, $P(H)$, were performed by using the constrained Hesse–Rübartsch method [30, 31]. The NORMOS program was used [32]. All isomer shifts are related to the α-Fe standard.

The Mössbauer experiments were supplemented by x-ray diffraction measurements. XRD was used for characterization of the as-deposited samples (see [19]) and for monitoring the formation of the amorphous phase due to ion irradiation. XRD measurements were carried out in the Bragg–Brentano geometry using Co Kα radiation.

3. Results and discussion

3.1. As-deposited Fe/Ti multilayers

The structure and magnetic properties of the as-deposited Fe/Ti multilayer (ML) samples have been described in detail elsewhere [19]. The as-deposited Fe/Ti MLs with $\beta = 1$ and 1.5 and $\Lambda = 10$ and 20 nm consist of predominantly crystalline close packed bcc (110) planes of Fe and (100) hcp Ti. The plane spacings, determined by XRD, were 0.2028 and 0.2558 nm for Fe and Ti, respectively [19]. The CEMS spectra of the film with $\Lambda = 10$ nm (figure 1(a)) and 20 nm consist of three spectral components:

(1) a sextet with $H_{\rm hf} \approx 32.9$ T and IS $= 0.00$ mm s^{-1} corresponding to the bcc-Fe layers,
(2) a broad sextet with $H_{\rm hf} \approx 29$ T and IS $= 0.00$ mm s^{-1} corresponding to the interfacial crystalline regions, most probably bcc-FeTi, and
(3) a quadrupole doublet with the quadrupole splitting QS ≈ 0.40 mm s^{-1} and IS ≈ -0.09 mm s^{-1}, corresponding to the amorphous iron-poor FeTi phase.

The spectral contributions of components (2) and (3) decrease with increasing elemental layer thickness (increasing Λ). The samples with thicker elemental layers ($\beta = 1$ and $\Lambda = 40$ nm (figure 1(g)) and $\Lambda = 60$ nm) are almost completely crystalline. Their CEMS spectra consist of the dominating Fe-sextet and the contribution of the QS doublet does not exceed 3% of the total spectral area (figures 1(g), 2(g)). The spectrum of the $\beta = 1.5$ sample with $\Lambda = 40$ nm still contains spectral components (2) and (3), figure 5(g), but the $\Lambda = 60$ nm sample is completely crystalline: the corresponding CEMS spectrum reveals the bcc-Fe sextet only.

3.2. Irradiations of the $\beta = 1$ samples with Ar and Kr ions

The fluence dependence of the ion-beam mixing was studied for $\beta = 1$ Fe/Ti multilayers with $\Lambda = 10$ and 40 nm and with $\Lambda = 20$ and 60 nm. These two sets of samples were irradiated with Ar or Kr ions in separate irradiation sessions. The examples of CEMS spectra are shown in figure 1 for Ar-irradiations and in figure 2 for Kr-irradiations. The relative fractions of various phases detected in CEMS spectra versus $\Phi^{1/2}$ are shown in figures 3 and 4 for Ar- and Kr-irradiations, respectively. As can be seen from figures 1(a) to (f), the irradiation with low fluence of Ar ions (up to 7.5×10^{14} Ar cm^{-2}) already induces severe mixing as a result of which new phases appear. The CEMS spectra were fitted with two fitting methods, depending on the shape of the given spectrum. At low Ar-ion fluence, when the spectra consist of two sextets ($H_{\rm hf1} \approx 32.9$ T, corresponding to bcc-Fe layers, and $H_{\rm hf2} \approx 30$ T,

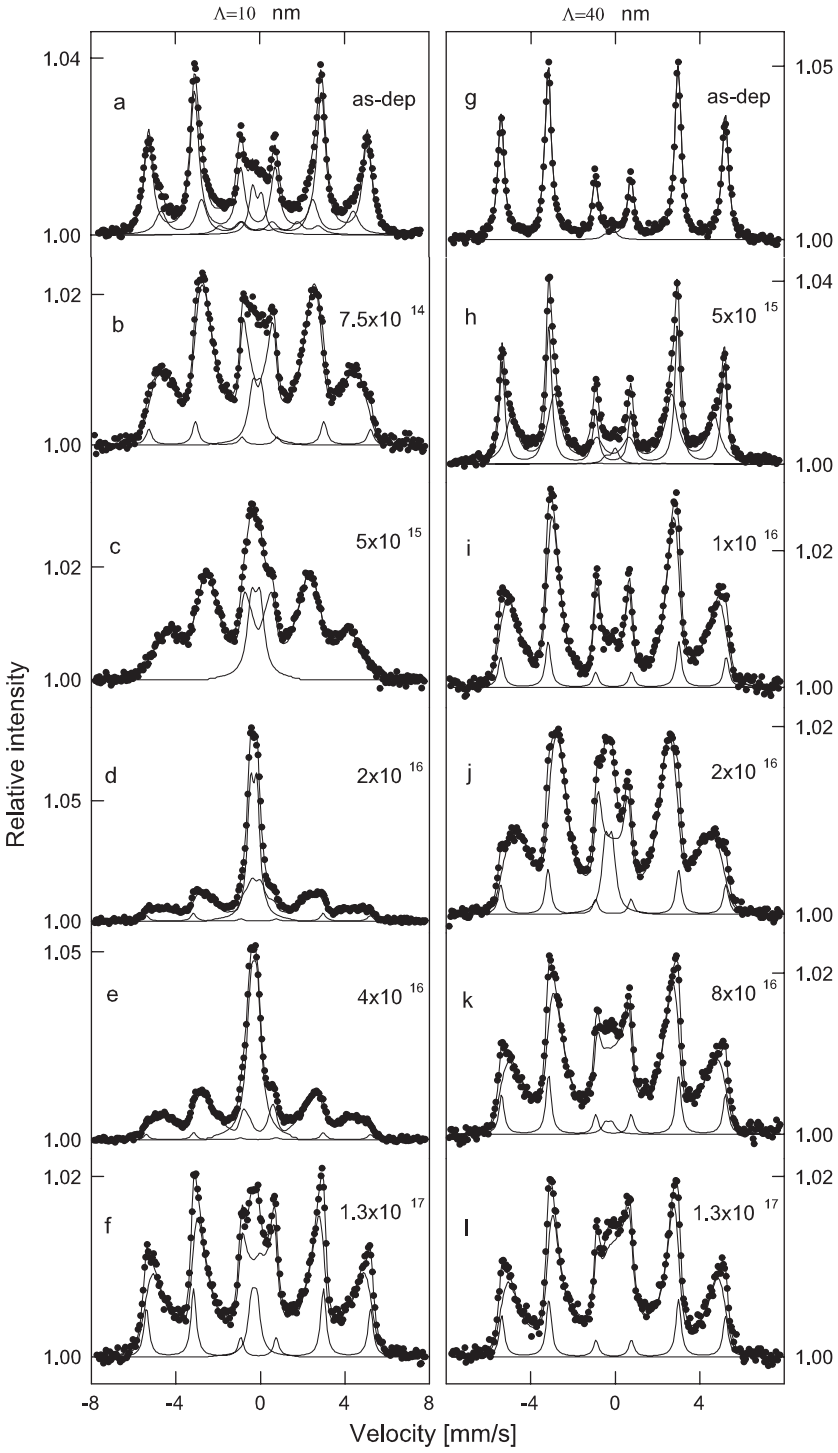

Figure 1. CEMS spectra measured as a function of Ar-ion fluence for Fe/Ti multilayers ($\beta = 1$) with $\Lambda = 10$ nm ((a)–(f)) and $\Lambda = 40$ nm ((g)–(l)).

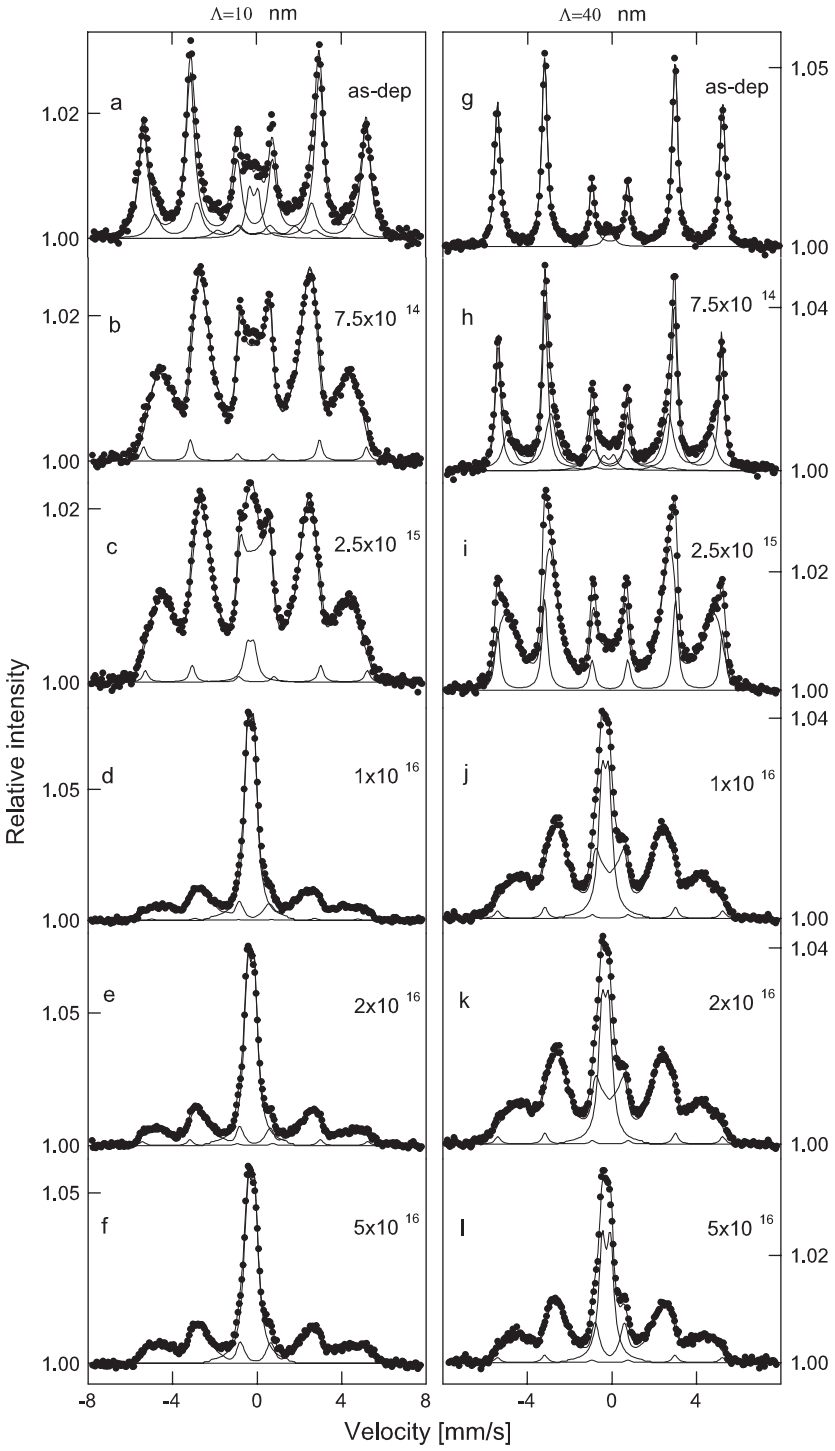

Figure 2. CEMS spectra measured as a function of Kr-ion fluence for Fe/Ti multilayers ($\beta = 1$) with $\Lambda = 10$ nm ((a)–(f)) and $\Lambda = 40$ nm ((g)–(l)).

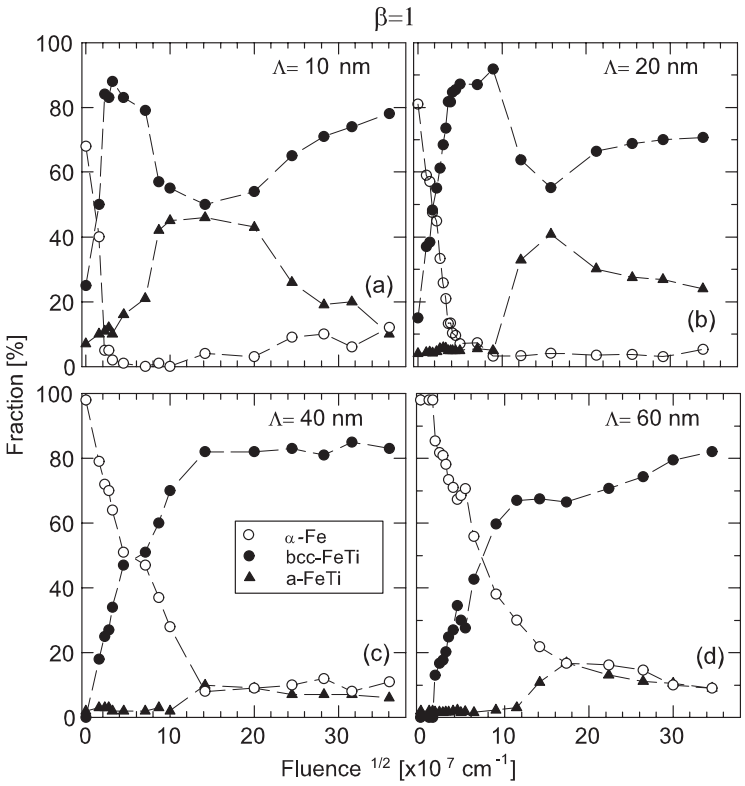

Figure 3. Phase abundance versus (fluence)$^{1/2}$ determined for Ar-ion-beam mixed Fe/Ti multilayers ($\beta = 1$) with $\Lambda = 10$ nm (a), 20 nm (b), 40 nm (c) and 60 nm (d).

corresponding to the interfacial bcc-FeTi solid solution) and a QS doublet corresponding to the amorphous FeTi phase, they were decomposed into three well-defined spectral components. However, with increasing Ar-ion fluence the fraction of the bcc-FeTi solid solution increased so much that the CEMS spectrum consisted of a dominating broad sextet accompanied by the residual bcc-Fe sextet with narrow lines and the QS doublet (figure 1(b)). Such a spectrum was fitted using the hyperfine field distribution component (corresponding to the bcc-FeTi solid solution) with additional discrete components due to bcc-Fe and amorphous FeTi phases. The fit revealed that at fluences of 2.5×10^{14} to 1×10^{15} Ar cm^{-2} the relative fraction of the bcc-FeTi solid solution reaches 87% at the expense of the bcc-Fe sextet that almost vanishes (relative fraction of about 2%). With the further increase of the Ar-ion fluence the QS doublet increases significantly, showing that the amorphization process becomes more effective (figure 1(c)). The amorphous FeTi phase contributes about 45% to the total spectral area for Ar-ion fluences of 1×10^{16}–4×10^{16} Ar cm^{-2} (figures 1(d), (e)) and then rapidly decreases to 10% only at a fluence of 1.3×10^{17} Ar cm^{-2}. The bcc-FeTi solid solution phase is greatly restored and its relative fraction increases to about 80% (figure 1(f)). Also the bcc-Fe sextet reappears at 4×10^{16} Ar cm^{-2} and its relative fraction increases up to 12% at the highest Ar-ion fluence used (figure 1(f)).

For larger thicknesses of layers ($\Lambda = 40$ nm, figure 1) the qualitative changes of the spectral shapes are similar. However, much higher ion fluence is necessary to achieve a similar mixing effect as for the $\Lambda = 10$ nm film. For example, the bcc-FeTi phase reaches its maximum abundance at 1×10^{16} Ar cm^{-2} (figure 1(i)) as compared with 1×10^{15} Ar cm^{-2} in the case of

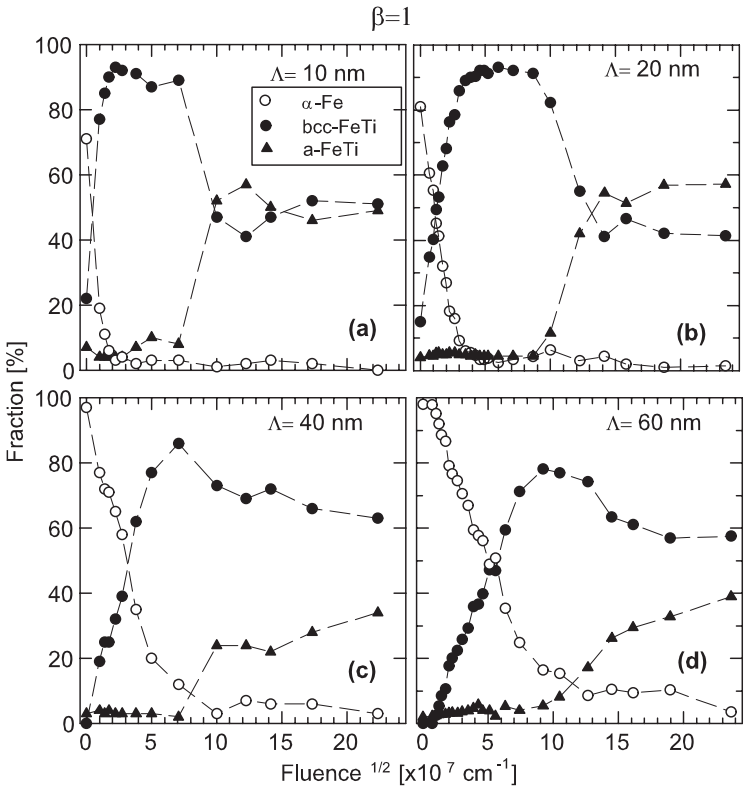

Figure 4. Phase abundance versus (fluence)$^{1/2}$ determined for Kr-ion-beam mixed Fe/Ti multilayers ($\beta = 1$) with $\Lambda = 10$ nm (a), 20 nm (b), 40 nm (c) and 60 nm (d).

the sample with $\Lambda = 10$ nm. The bcc-FeTi phase dominates strongly for all Ar-ion fluences exceeding 1×10^{16} Ar cm^{-2}; its relative fraction remains almost constant (82–85%) for the fluence range 2×10^{16}–1.3×10^{17} Ar cm^{-2} (figures 1(j)–(l)). The bcc-Fe component decreases strongly with increasing Ar-ion fluence, especially for low fluences. Its relative fraction decreases from 79% at 2.5×10^{14} Ar cm^{-2} to about 10% at 1×10^{16} Ar cm^{-2} (figure 1(i)) and remains almost unchanged for the high fluence range (figures 1(j)–(l)). The spectral component related to the amorphous phase reaches its maximum of 10% in the fluence range 2×10^{16}–4×10^{16} Ar cm^{-2} and then decreases for the highest Ar-ion fluences (figures 1(k), (l)). This decrease is, however, not that dramatic as in the case of the $\Lambda = 10$ nm sample, discussed above.

The fluence dependence of ion-beam mixing observed for two other samples ($\Lambda = 20$ nm and $\Lambda = 60$ nm) irradiated in separate irradiation runs reveals similar features. Especially spectacular transformation of the crystalline Fe and Ti layers into the bcc-FeTi solid solution phase is observed for $\Lambda = 20$ nm multilayers irradiated with 8×10^{15} Ar cm^{-2}. The spectrum of the film irradiated with 8×10^{15} Ar cm^{-2} consists almost exclusively of the broad sextet (due to the hyperfine field distribution); the relative spectral contribution of the bcc-Fe sextet is only about 2%, and the QS doublet does not exceed 5%. The shape of the spectra does not change for a fluence range of 1.5×10^{15}–8×10^{15} Ar cm^{-2}. The increase of the Ar-fluence to 1.5×10^{16} Ar cm^{-2} induces a sudden change in the phase composition. The amorphous phase is rapidly formed at about 1.5×10^{16} Ar cm^{-2}. The spectral contribution of the QS doublet increases from 5% at 8×10^{15} Ar cm^{-2} to 32% at 1.5×10^{16} Ar cm^{-2}. The spectral contribution of the QS doublet reaches a maximum (40%) at 2.5×10^{16} Ar cm^{-2} and then

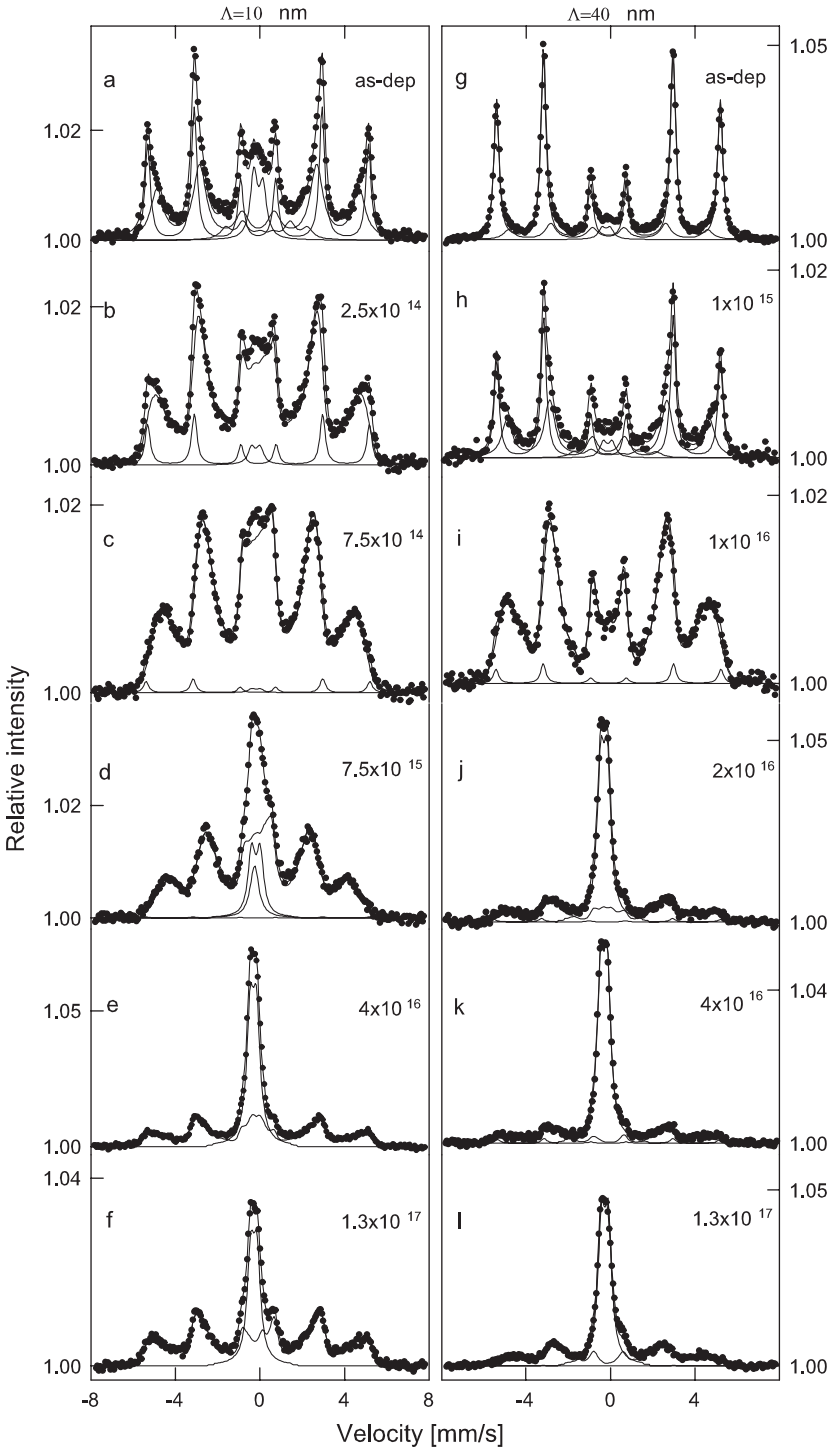

Figure 5. CEMS spectra measured as a function of Ar-ion fluence for Fe/Ti multilayers ($\beta = 1.5$) with $\Lambda = 10$ nm ((a)–(f)) and $\Lambda = 40$ nm ((g)–(l)).

decreases markedly to 24% at 1.15×10^{17} Ar cm^{-2}. Similarly to the sample with $\Lambda = 10$ nm, the bcc-FeTi component is partially restored at highest Ar-ion fluences.

The sample with the thickest elemental layers of 30/30 nm Fe/Ti ($\Lambda = 60$ nm) behaves in a similar way to that with $\Lambda = 40$ nm (figures 1(g)–(l)). Again, the amorphous phase appears at about 1.6×10^{16} Ar cm^{-2}, reaches its maximum abundance at about 3×10^{16} Ar cm^{-2} and decreases at the highest Ar-ion fluences.

Irradiation with Kr ions induces a similar structural transformation of Fe/Ti multilayers with $\beta = 1$ and $\Lambda = 10$, 40 nm (figure 2) and 20 and 60 nm. At low ion fluences the ion-beam mixing leads to the formation of the bcc-FeTi solid solution at the expense of the initial crystalline layers of Fe and Ti. Almost complete transformation of Fe layers into the bcc-FeTi phase occurs at markedly lower ion fluences as compared with the Ar-ion irradiations. Considerably higher Kr-ion fluences are required to induce a similar degree of mixing in the multilayers with larger Λ. The abundance of the bcc-FeTi phase saturates at about 90–93% at $\Phi = 3 \times 10^{14}$–5×10^{15} Kr cm^{-2} for $\Lambda = 10$ nm and at $\Phi = 1.2 \times 10^{15}$–$1 \times 10^{16}$ Kr cm^{-2} for $\Lambda = 20$ nm. When the Kr-ion fluence exceeds these upper fluence limits a sudden formation of the amorphous FeTi phase occurs, as evidenced by the rapid increase of the spectral component consisting of the QS doublet from 8% at 5×10^{15} Kr cm^{-2} to 52% for a fluence of 1×10^{16} Kr cm^{-2} for $\Lambda = 10$ nm (figure 2(d)) and from 5% at 7.5×10^{15} Kr cm^{-2} to 42% at 1.5×10^{16} Kr cm^{-2} and 54% at 2×10^{16} Kr cm^{-2} for $\Lambda = 20$ nm. The decrease of the QS fraction for the highest Kr-ion fluences is only marginal. For larger Fe and Ti layers thicknesses ($\Lambda = 40$ and 60 nm) the mixing induced by heavier ions (Kr) is considerably stronger than in the case of Ar ions and the amorphization process is more effective in the entire Kr fluence range studied. The amorphous phase is more abundant in films with $\Lambda = 40$ nm (figures 2(j)–(l)) and 60 nm at high Kr doses as compared with that observed for the Ar-irradiated samples (figures 1(j)–(l)). Its relative fraction reaches almost 40% for $\Lambda = 60$ nm while it did not exceed 15% for the corresponding Fe/Ti MLs irradiated with Ar-ions.

The results discussed above are summarized in figures 3 and 4 for Ar- and Kr-irradiated Fe/Ti MLs with $\beta = 1$, respectively, and all the details of the structural transformations discussed above are clearly seen. It can be seen that in the MLs with $\Lambda = 10$ and 20 nm irradiated both with Ar and Kr ions the onset of the transformation from the crystalline to amorphous phase occurs suddenly. At low ion fluences the original crystalline Fe and Ti layers are mixed at the interfaces and are converted into bcc-FeTi solid solution, the relative fraction of which increases almost linearly versus $\Phi^{1/2}$ (figures 3(a), (b) and 4(a), (b)). Then there is a well-defined fluence range in which this phase reaches its maximum abundance and saturates. The starting α-Fe phase vanishes almost completely; entire Fe layers are consumed for the formation of the solid solution FeTi phase. The increase of the ion fluence over a certain threshold fluence, which depends on Λ and the type of ion, induces rapid transformation of the bcc-FeTi solid solution into amorphous FeTi phase. The relative fraction of the broad sextet related to the bcc-FeTi phase suddenly decreases and the QS doublet emerges (figures 3(a), (b) and 4(a), (b)). The relative content of the amorphous phase reaches its maximum of about 50% for Ar-irradiated samples (figures 3(a), (b)) and then markedly decreases; the bcc-FeTi phase is partly restored. The Kr-ion irradiation also leads to rapid formation of the amorphous phase, whose relative fraction reaches almost 60% (figures 4(a), (b)) but the decrease of its content for the highest Kr-fluences is only marginal, in clear distinction to the Ar-ion irradiations.

In samples with larger Λ ($\Lambda = 40$ and 60 nm, figures 3(c) and (d)) irradiated with lighter ions (Ar) the amorphization process is only marginal. The ion-beam irradiation effectively mixes the Fe and Ti layers and transforms them into solid solution bcc-FeTi which dominates for all Ar-ion fluences exceeding 5×10^{15} Ar cm^{-2} (figures 3(c), (d)). The amorphous phase appears at the expense of the remaining Fe layer rather than at the expense of the bcc-FeTi

phase (figures 3(c), (d)), in distinction to the $\Lambda = 10$ nm and $\Lambda = 20$ nm samples (figures 3(a) and (b)). The picture is different for the Kr-irradiated samples with $\Lambda = 40$ and 60 nm (figures 4(c), (d)). In the latter case the amorphous phase is formed at the expense of the bcc-FeTi solid solution. Most probably, the original Fe layers are almost completely consumed for the formation of the bcc-FeTi phase, while in the case of the Ar-irradiated samples a significant fraction of thick Fe layer was not converted into the solid solution phase. The amount of the amorphous FeTi phase still increases for the highest Kr-ion fluences (figures 4(c), (d)).

In all cases the effective amorphization process starts when the relative fraction of the bcc-FeTi phase is saturated. Thus, the amorphization process induced by the ion-beam mixing in Fe/Ti MLs is most effective after the original Fe and Ti layers are mixed into bcc-FeTi solid solution, in clear distinction to the case of Fe/Zr multilayers with similar modulation wavelengths studied recently [33], in which the amorphous FeZr phase is formed directly from the original Fe and Zr layers without the intermediate crystalline solid solution phase.

3.3. Ar and Kr irradiations of the samples with $\beta = 1.5$

The CEMS spectra typical for low, intermediate and high fluence ranges, recorded for multilayers with $\beta = 1.5$ and $\Lambda = 10$ and 40 nm irradiated with Ar and Kr ions are shown in figures 5 and 6, respectively. The qualitative changes observed in the spectra in figures 5 and 6 are quite similar to those obtained for $\beta = 1$ samples discussed above. At low ion fluences the ion-beam mixing leads to the formation of the bcc-FeTi phase which in the samples with the smallest thicknesses of Fe and Ti layers (4/6 nm) rapidly reaches its maximum abundance of 89% at only 5×10^{14} Ar cm^{-2} (figures 5(b), (c)) and at 2×10^{14} Kr cm^{-2} (figure 6(b)). The relative fraction of this phase saturates at 88% for a fairly wide fluence range (2.4×10^{14}–5×10^{15} Ar cm^{-2}, figures 5(b), (c), and 2×10^{14}–7.5×10^{14} Kr cm^{-2}, figures 6(b), (c)). At about 7.5×10^{15} Ar cm^{-2} and 1.45×10^{15} Kr cm^{-2} the amorphous FeTi phase forms rapidly, as evidenced by the strong increase of the relative spectral area of the QS doublet (figures 5(d) and 6(d)). The relative fraction of the amorphous phase reaches its maximum of about 60% at 4×10^{16} Ar cm^{-2} (figure 5(e)) and 71% at 1–2 $\times 10^{16}$ Kr cm^{-2} (figure 6(e)). Further increase of the Ar-ion fluence leads to the gradual decrease of the amorphous fraction; the relative spectral area of the QS doublet decreases to only 29% at 1.3×10^{17} Ar cm^{-2} (figure 5(f)) in a similar way as discussed above for the sample with $\Lambda = 10$ nm and $\beta = 1$ (figure 1). The bcc-FeTi solid solution phase is partly restored (relative fraction of 71%, figure 5(e)) but no restoration of the α-Fe was observed.

The Kr-ion irradiation leads to the formation of a more stable amorphous FeTi phase. In the sample with $\Lambda = 10$ nm the relative fraction of the amorphous phase remains almost constant (71%, figure 6(e)) and it starts to decrease slightly (to 66%) at the highest Kr-ion fluence used (5×10^{16} Kr cm^{-2}), figure 6(f).

The structural transformations observed in the ML films with thicker Fe and Ti layers ($\Lambda = 40$ nm, $\beta = 1.5$) are qualitatively similar to those observed in figures 5(a)–(f) and 6(a)–(f). However, in order to obtain the same mixing effect (i.e., the same relative fraction of the bcc-FeTi phase) a higher fluence of Ar or Kr ions must be used. For example, the relative amount of the bcc-FeTi phase increases gradually with increasing Ar-ion fluence and reaches its maximum content of 93% at 1×10^{16} Ar cm^{-2} (figure 5(i)) and the amorphous phase appears suddenly at 2×10^{16} Ar cm^{-2} (figure 5(j)). The relative spectral area of the QS doublet increases from 3% at 1×10^{16} Ar cm^{-2} (figure 5(i)) to 63% at 2×10^{16} Ar cm^{-2} (figure 5(j)) and saturates at 70% for the dose range of 4×10^{16}–1×10^{17} Ar cm^{-2} (figure 5(k)). Only at the highest Ar fluence does the relative fraction of the amorphous phase start to decrease (to 57% at 1.3×10^{17} Ar cm^{-2}, figure 5(l)).

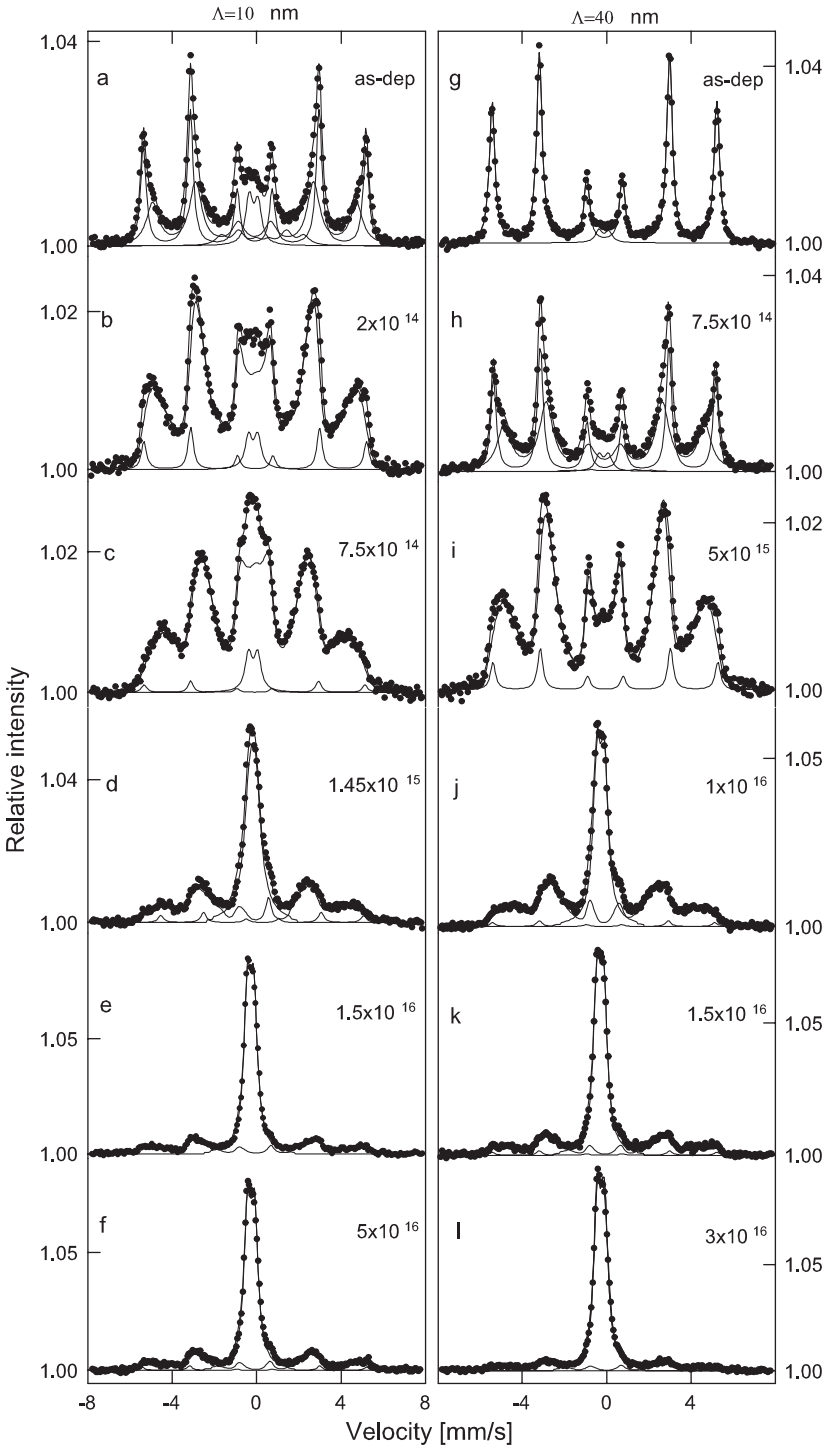

Figure 6. CEMS spectra measured as a function of Kr-ion fluence for Fe/Ti multilayers ($\beta = 1.5$) with $\Lambda = 10$ nm ((a)–(f)) and $\Lambda = 40$ nm ((g)–(l)).

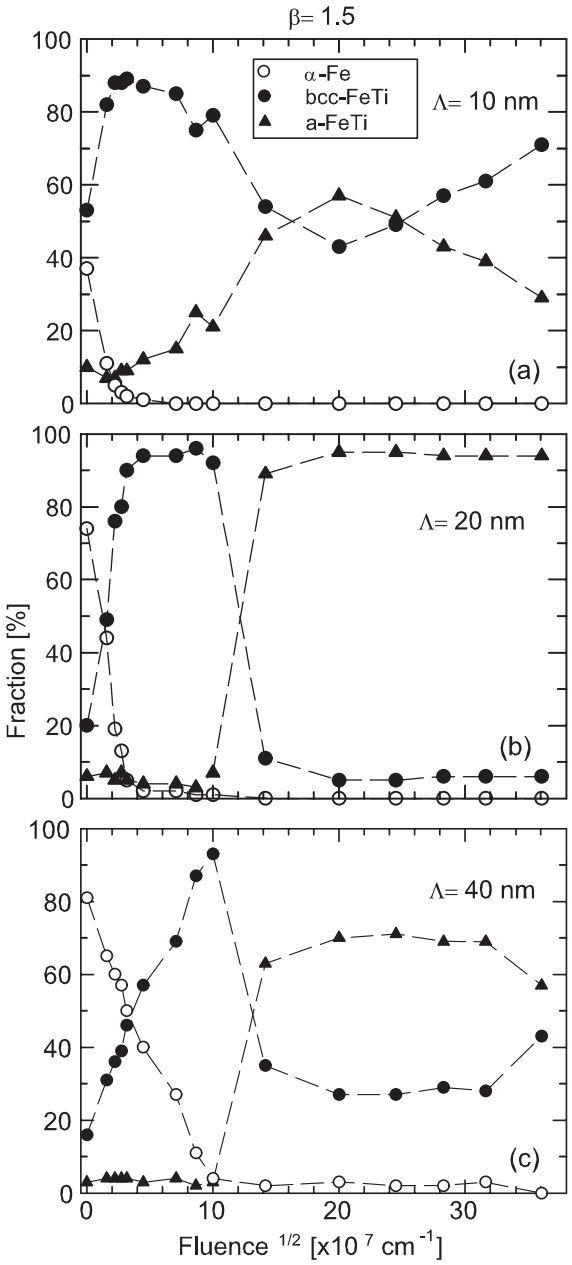

Figure 7. Phase abundance versus (fluence)$^{1/2}$ determined for Ar-ion-beam mixed Fe/Ti multilayers ($\beta = 1.5$) with $\Lambda = 10$ nm (a), 20 nm (b) and 40 nm (c).

The amorphous FeTi phase appears suddenly in a similar sample irradiated with Kr ions at 1×10^{16} Kr cm^{-2} (figure 6(j)). Its relative fraction increases to 80% with Kr-ion fluence increasing to 3×10^{16} Kr cm^{-2} (figure 6(l)). Even at such a high Kr-ion fluence the effect of the partial restoration of the bcc-FeTi phase is not observed, in contrast to the case shown in figure 5(l).

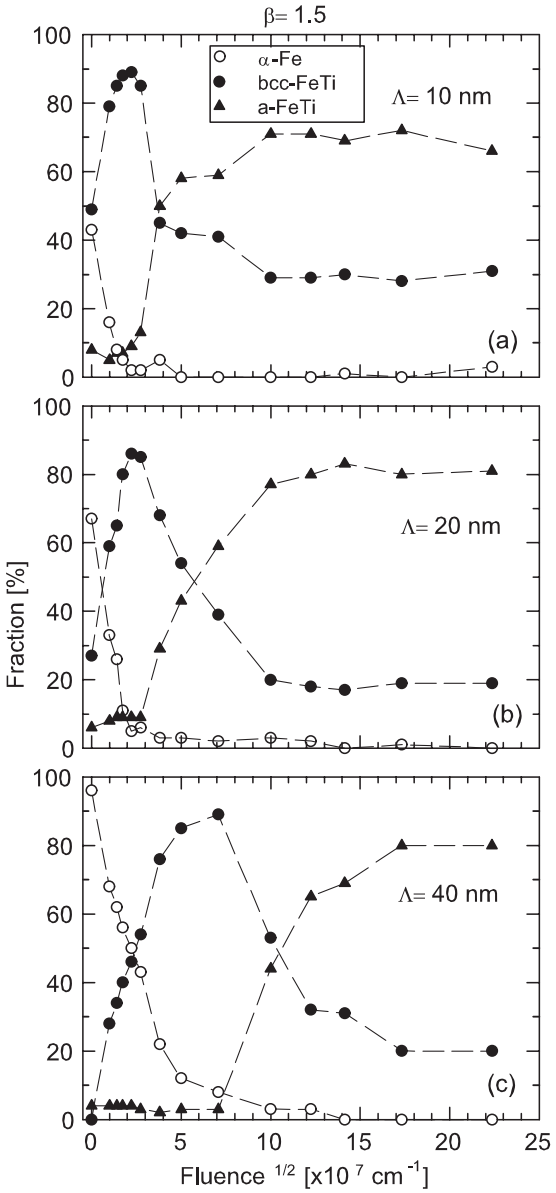

Figure 8. Phase abundance versus (fluence)$^{1/2}$ determined for Kr-ion-beam mixed Fe/Ti multilayers ($\beta = 1.5$) with $\Lambda = 10$ nm (a), 20 nm (b) and 40 nm (c).

The relative fractions of the bcc-Fe, bcc-FeTi and amorphous FeTi phases versus $\Phi^{1/2}$ and their changes discussed above are collected in figures 7 and 8 for Ar- and Kr-ion irradiations, respectively.

The results discussed above can be summarized as follows (figures 7 and 8): at low ion fluences the ion-beam mixing induces structural transformation consisting in the consumption of the starting crystalline Fe and Ti layers that leads to the formation of the bcc-FeTi solid solution. In the medium ion fluence range the relative abundance of this phase saturates at

almost 90%. The spectral component related to the α-Fe layers disappears even in the sample with $\Lambda = 40$ nm. Further increase of the ion fluence induces sudden structural transformation of the bcc-FeTi phase to amorphous FeTi. The amorphous phase is formed at the expense of the bcc-FeTi phase. The amorphous phase dominates at high ion fluences but in thin Fe/Ti MLs ($\Lambda = 10$ nm) irradiated with fluences exceeding 8×10^{16} Ar cm^{-2} its relative abundance markedly decreases for the highest ion fluences used and causes a partial restoration of the bcc-FeTi phase (figure 7(a)). This effect is much less pronounced in the $\Lambda = 40$ nm sample (figure 7(c)) and is not observed in the Kr-irradiated samples (figure 8).

4. Discussion

Our detailed and systematic study of the structural transformations induced in Fe/Ti multilayers by Ar or Kr ion-beam mixing leads to the following findings. The increase of the relative fraction of the bcc-FeTi phase at low ion fluences is almost linear versus $\Phi^{1/2}$ for all samples studied (figures 3, 4, 7, 8). This suggests that the mass transport during mixing occurs due to a 'random walk' mechanism and that the chemical forces play a minor role. The structural transformations and the changes of the relative fractions of the relevant phases can be associated with the changes of the iron content in the mixed phases. As shown in [22], the enthalpy curves for the amorphous FeTi and bcc-FeTi solid solution show three ranges for the stability of these phases depending on the Fe content, x:

(1) a single amorphous state for $0.36 < x < 0.72$,
(2) two phases, bcc-FeTi and amorphous FeTi, can exist for $0.10 < x < 0.36$, and
(3) a single bcc-FeTi phase exists for $x < 0.10$ and $x > 0.81$.

We observed in our study the formation of the bcc-FeTi phase in MLs with small Λ ($\Lambda = 10$, 20 nm) at low ion fluences. Its increase up to the saturation level (figures 3, 4) is related to a complete consumption of the starting α-Fe layers by the formation of the bcc-FeTi solid solution. An increase of ion fluence does not affect the iron content in the solid solution but further increase of the ion fluence causes an increase of the lattice strain in the bcc structure. The amorphous phase appears rapidly when the strain becomes sufficiently large [34]. The formation of this phase releases the strain. However, further increase of ion fluence causes a decrease of the amorphous fraction and partial restoration of the bcc-FeTi fraction (figures 3(a), (b)). This effect is not fully understood at the moment. It may be related to a partial segregation of Ti from the bcc phase (e.g. due to the formation of TiC with carbon contamination) that would cause an increase of iron content in the solid solution sufficient for the transition from the iron range (2) in the direction of range (3) or to the formation of the noble gas bubbles that leads to stress release.

From the relative fraction of the mixed phase it is possible to estimate the average thickness of the iron layer converted into the bcc-FeTi phase. The mixed layer thickness is $\Delta x = nd\Delta F/2$, where n is the number of monolayers of Fe per Fe–Ti bilayer, $d = 0.2028$ nm (d spacing in the Fe layer), ΔF is the spectral area fraction of a given phase and the factor 2 accounts for two Fe–Ti interfaces per Fe layer [33]. The thickness of the Fe layer converted into the bcc-FeTi phase when it reaches its maximum abundance estimated in this way for MLs with $\Lambda = 60$ nm irradiated with 1.3×10^{16} Ar cm^{-2} is about 10 nm. A similar estimation for $\Lambda = 20$ nm shows that entire Fe layers are consumed for the formation of the bcc-FeTi phase. The 3% spectral contribution of the α-Fe component results most probably from deep Fe layers in the ML film, beyond the range of Ar or Kr ions. A similar estimation for $\Lambda = 60$ nm ML irradiated with 8.5×10^{15} Kr cm^{-2} gives $\Delta x \cong 11.7$ nm.

It is worth noting that the relative fractions of the mixed phases (bcc-FeTi and amorphous FeTi) are, for a given β, considerably larger in MLs with small Λ despite the fact that the nominal compositions of our MLs with the same β and different Λ are the same. Therefore not only does the nominal composition of the ML structure determine the formation of a given phase, but the thickness of the elemental layers in the starting system is also important.

The ion-beam mixing of Fe/Ti MLs is very sensitive to the contamination of the Fe/Ti system by carbon or oxygen. As was shown by Brenier *et al* [23], such a contamination can prevent the formation of the amorphous phase. However, in cleaner Fe/Ti MLs the amorphization effect due to Xe ion-beam mixing was reported [22]. All our samples were prepared in the same deposition conditions, therefore it is expected that the possible contamination of the Fe–Ti interfaces remains at the same level and does not significantly affect the dependence of the structural transformations on the type of ion, ion fluence, sample composition (β) and elemental thickness Λ of Fe and Ti discussed above.

In summary, the experiments described here allowed us to determine qualitatively the phase transformations induced in the Fe/Ti multilayer system by irradiation with noble gas ions, Ar and Kr. The results point to a complex sequence of transformations depending on composition, thickness of sublayers and purity of the deposited Fe/Ti multilayers. The formation of the amorphous Fe–Ti phase is most probably related to the stress induced by the incorporation of foreign atoms.

References

[1] Johnson W L, Cheng Y T, Van Rossum M and Nicolet M A 1985 *Nucl. Instrum. Methods* B **7/8** 657
[2] Pain B and Averback R S 1985 *Nucl. Instrum. Methods* B **7/8** 666
[3] Cheng Y T 1990 *Mater. Sci. Rep.* **5** 45
[4] Okamoto P R, Lam N Q and Rehn L E 1999 *Solid State Phys.* **52** 1
[5] Jagielski J, Thome L and Benkoulal T 1994 *Phys. Rev.* B **50** 2815
[6] Sigmund P and Gras-Marti A 1980 *Nucl. Instrum. Methods* **168** 389
Sigmund P and Gras-Marti A 1981 *Nucl. Instrum. Methods* **182/183** 25
[7] Borgesen P, Lilienfeld D A and Johnson H H 1990 *Appl. Phys. Lett.* **57** 1407
[8] Lam N Q, Okamoto P R and Johnson R A 1978 *J. Nucl. Mater.* **78** 408
[9] Liu B X, Wilson W L, Nicolet M A and Lau S S 1984 *Nucl. Instrum. Methods* **209/210** 229
[10] Wertheim G K, Wernick J H and Sherwood R C 1969 *Solid State Commun.* **7** 1399
[11] Mizuno T and Morozuni T 1982 *J. Less-Common. Met.* **84** 237
[12] Murray J L 1986 *Binary Alloy Phase Diagrams* vol 2, ed T B Massalski (Metals Park, OH: American Society for Metals) p 1117
[13] Sumiyama K, Hashimoto Y, Yoshikate T and Nakamura Y 1983 *J. Magn. Magn. Mater.* **31–34** 1495
[14] Liou S and Chien C L 1984 *J. Appl. Phys.* **55** 1820
[15] Chien C L and Liou S 1985 *Phys. Rev.* B **31** 8238
[16] Rodmacq B, Hillairet J, Laugier J and Chamberod A 1990 *J. Phys.: Condens. Matter* **2** 95
[17] Balogh J, Rodmacq B and Chamberod A 1988 *Solid State Commun.* **66** 143
[18] Ray R, Giessen B C and Grant N J 1972 *Metall. Trans.* **3** 627
[19] Kopcewicz M, Stobiecki T, Czapkiewicz M and Grabias A 1997 *J. Phys.: Condens. Matter* **9** 103
[20] Eckert J, Schulz L and Urban K 1991 *J. Non-Cryst. Solids* **127** 90
[21] Kopcewicz M, Jagielski J and Grabias A 2000 *J. Phys.: Condens. Matter* **12** 2297
[22] Brennier R, Capra T, Thevenard P, Perez A, Treilleux M, Rivory J, Dupuy J and Giraud G 1990 *Phys. Rev.* B **41** 11748
[23] Brennier R, Perez A, Thevenard P and Capra T 1985 *Mater. Sci. Eng.* **69** 83
[24] Nakatani R, Hoshino K, Noguchi S and Sugito Y 1994 *Japan. J. Appl. Phys.* **33** 133
[25] Maeland A J 1985 *Proc. 5th Int. Conf. on Rapidly Quenched Metals* ed S Steeb and H Warlimont (Amsterdam: North-Holland) p 1507
[26] Menzel D, Niklas A and Köster H 1991 *Mater. Sci. Eng.* A **133** 312
[27] Nakamura Y, Sumiyama K and Ezawa H 1986 *Hyperfine Interact.* **27** 361
[28] Kopcewicz M, Jagielski J, Gawlik G and Grabias A 1995 *J. Appl. Phys.* **78** 1312

[29] Biersack J P and Haggmark L G 1980 *Nucl. Instrum. Methods* **174** 257
[30] Hesse J and Rübartsch A 1974 *J. Phys. E: Sci. Instrum.* **7** 526
[31] LeCaer G and Dubois J M 1979 *J. Phys. E: Sci. Instrum.* **12** 1083
[32] Brand R A, Lauer J and Herlach D M 1983 *J. Phys. F: Met. Phys.* **13** 675
[33] Kopcewicz M, Jagielski J, Stobiecki T, Stobiecki F and Gawlik G 1994 *J. Appl. Phys.* **76** 5232
[34] Linker G 1987 *Nucl. Instrum. Methods* B **19/20** 526